

Instant Adversarial Purification with Adversarial Consistency Distillation

Chun Tong Lei¹, Hon Ming Yam¹, Zhongliang Guo², Chun Pong Lau¹

¹City University of Hong Kong

²University of St Andrews

{ctlei2, hmyam4, cplau27}@cityu.edu.hk, zg34@st-andrews.ac.uk

Abstract

Neural networks, despite their remarkable performance in widespread applications, including image classification, are also known to be vulnerable to subtle adversarial noise. Although some diffusion-based purification methods have been proposed, for example, DiffPure, those methods are time-consuming. In this paper, we propose One Step Control Purification (OSCP), a diffusion-based purification model that can purify the adversarial image in one Neural Function Evaluation (NFE) in diffusion models. We use Latent Consistency Model (LCM) and ControlNet for our one-step purification. OSCP is computationally friendly and time efficient compared to other diffusion-based purification methods; we achieve defense success rate of 74.19% on ImageNet, only requiring 0.1s for each purification. Moreover, there is a fundamental incongruence between consistency distillation and adversarial perturbation. To address this ontological dissonance, we propose Gaussian Adversarial Noise Distillation (GAND), a novel consistency distillation framework that facilitates a more nuanced reconciliation of the latent space dynamics, effectively bridging the natural and adversarial manifolds. Our experiments show that the GAND does not need a Full Fine Tune (FFT); PEFT, e.g., LoRA is sufficient.

Introduction

Deep Neural Networks (DNNs) have revolutionized the field of computer vision, achieving remarkable milestones across a spectrum of tasks. From the groundbreaking performance in image classification (Krizhevsky, Sutskever, and Hinton 2012; Simonyan and Zisserman 2015a; Yue and Li 2024) to significant advancements in object detection (Zhao et al. 2019; Huang et al. 2023), image segmentation (Girshick et al. 2014; Minaee et al. 2021) and face recognition (Liu et al. 2023a), DNNs have consistently pushed the boundaries of artificial intelligence. However, beneath this veneer of success lies a disconcerting vulnerability that has captured the attention of researchers worldwide (Lau et al. 2023a).

The Achilles' heel of these powerful models manifests in their susceptibility to adversarial attacks (Liu et al. 2022b). These attacks, orchestrated through the introduction of carefully crafted, imperceptible perturbations to input data, can manipulate DNNs into making egregious misclassifications (Liu et al. 2023b). Although some works have leveraged this weakness as a benign metric to prevent the underlying misuse of generative AI (Liu, Lau,

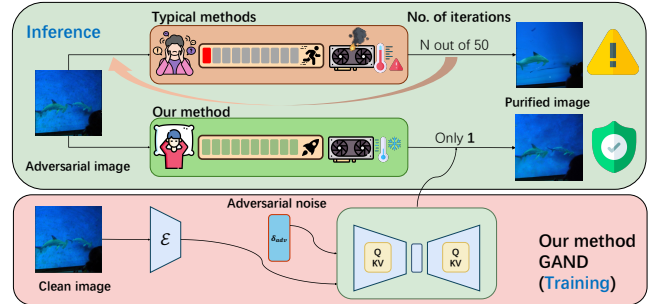


Figure 1: The comparison of existing methods and our proposed method. As illustrated, our method only requires 1 inference step, which is extremely fast compared to the previous. Moreover, we fine-tune our U-Net to adapt to adversarial noise. Our method serves as a computationally friendly robustness toolbox for adversarial purification.

and Chellappa 2023; Guo et al. 2024), the implications of this vulnerability extend far beyond academic interest, posing a formidable challenge to the deployment of DNNs in security-critical applications, where reliability and robustness are paramount (Souri et al. 2021).

In response to these challenges, two primary defense strategies have emerged: adversarial training (Tramer and Boneh 2019; Liu et al. 2022a; Wang et al. 2023) and adversarial purification (Samangouei, Kabkab, and Chellappa 2018; Yoon, Hwang, and Lee 2021; Nie et al. 2022). However, adversarial training faces significant limitations in practical applications. Adversarial training requires prior knowledge of attack methods to generate adversarial examples, which inherently limits its scope and effectiveness against unknown threats. In contrast, adversarial purification offers a more versatile defense mechanism. This approach provides a broader spectrum of protection without the need to anticipate specific attack methods. By focusing on removing adversarial perturbations rather than training against known attacks, purification methods offer a more generalized defense strategy, potentially more adaptable to the evolving landscape of adversarial threats.

Adversarial purification typically leverages generative models to achieve a distribution shift from adversarial samples back to benign ones. In this context, diffusion models

(Ho, Jain, and Abbeel 2020; Song, Meng, and Ermon 2021) have emerged as a particularly promising tool and achieved a good performance of anti-attack (Nie et al. 2022; Wang et al. 2022). These models offer significant advantages over other generative approaches, such as Generative Adversarial Networks (GANs), notably in terms of training stability and ease of implementation. The ability of diffusion models to generate high-quality samples by gradually denoising random noise has made them an attractive choice for adversarial purification.

However, diffusion models face a critical limitation that hinders their practical application. The inference process of these models involves multiple denoising steps, resulting in a computationally intensive and time-consuming operation. This inherent slowness poses a significant challenge, particularly in contexts where rapid response times are crucial, such as real-time image classification or security systems. The computational overhead of diffusion models severely restricts their applicability in scenarios demanding swift adversarial defenses, creating a pressing need for more efficient purification methods that can maintain the quality of defense while significantly reducing computational cost.

To address these challenges, we propose One Step Control Purification (OSCP), a novel diffusion-based purification method that requires only a single inference step. Our approach ingeniously combines the concept of consistency distillation with a nuanced consideration of the disparities between adversarial and clean samples. This synthesis culminates in our innovative Gaussian Adversarial Noise Distillation (GAND) framework, which achieves effective purification in just one inference step, dramatically reducing computational overhead while maintaining robust defense capabilities.

We tackle a long-standing issue in diffusion-based methods: semantic information losses when a large diffusion step is chosen. This problem is compounded by Latent Consistency Models, which make the trade-off between speed and semantic integrity, can result in blurry images. To overcome these limitations, we introduce a Controlled Adversarial Purification method (CAP), which utilizes ControlNet and Canny Edge detector to produce a clear purified image while maintaining most of the semantic information.

Our OSCP method, integrated by both GAND and CAP, achieving 74.19% robust accuracy on ImageNet using only 0.1s for each purification, represents a significant advancement in the field of adversarial purification. By addressing the critical issues of computational efficiency and semantic information loss, we pave the way for more practical and effective defenses against adversarial attacks in real-world applications.

In summary, our contribution can be summarized as:

- We proposed a novel consistency distillation method GAND for adversarial training on LCM. Empirical shows GAND has remarkable transferability on unknown attacks.
- We introduce CAP, a novel framework utilizing non-learnable edge detection operators to enhance adversarial purification controllability.

- OSCP combines CAP and GAND, achieving rapid purification process, which extends diffusion base purification to real time.

Related Work

Adversarial training Adversarial training (Madry et al. 2018) has emerged as one of the most effective methods for enhancing the robustness of DNNs against adversarial attacks by incorporating adversarial examples into the training process (Lau et al. 2023b). The impressive performance (Athalye, Carlini, and Wagner 2018; Goyal et al. 2020; Rebuffi et al. 2021) highlights its ability to significantly enhance the resilience of DNNs to various known attacks. Despite its success, adversarial training tends to overfit these specific perturbations, potentially limiting the robustness of novel attacks (Lin et al. 2020). To address this, recent adversarial training is trying to make use of the diffusion model to generate more image data for adversarial training (Tramer and Boneh 2019; Goyal et al. 2021; Wang et al. 2023), to prevent overfitting to the adversarial images.

Adversarial Purification Adversarial purification is a method that purifies images before classification. At first, GAN model is used to purify adversarial noise (Samangouei, Kabkab, and Chellappa 2018), then after the significant performance of the diffusion models. Diffusion models (Song and Ermon 2019; Ho, Jain, and Abbeel 2020; Song, Meng, and Ermon 2021) are used to purify noisy images, showing a remarkable performance (Yoon, Hwang, and Lee 2021; Nie et al. 2022; Wang et al. 2022). Removing the adversarial noise from the mixture of adversarial noise and Gaussian noise from the forward process simultaneously, Diff-Pure (Nie et al. 2022) claims that following forward diffusion, the KL divergence between the distributions of clean and adversarial images is reduced. This indicates a more aligned and purified output. However, a notable challenge remains the prolonged purification process, which can be inefficient and impractical (Wang et al. 2022).

Diffusion model Diffusion models have promising performance in various fields, such as text-to-image generation (Rombach et al. 2022; Saharia et al. 2022), video generation (Ho et al. 2022; Blattmann et al. 2023) and 3D generation (Luo and Hu 2021; Poole et al. 2023). Denoising Diffusion Probabilistic Models (DDPM) (Ho, Jain, and Abbeel 2020) is proposed as an image-to-image model, diffusing the original image by Gaussian noise, noted as forward process, which satisfies Markov property. Then, the model recovers the image by learning the reverse Markov chain, noted as reverse process. However, the inference time is incredibly long since the time is correlated to number of inference steps. Consistency Model (Song et al. 2023) adds a consistency constraint to Diffusion models, aiming to generate the image in a few inference steps. After that, Latent Consistency Model (LCM) (Luo et al. 2023a) is invented to speed up the generating process further. In LCM-LoRA (Luo et al. 2023b), using Low Rank Adaptation (LoRA), a Parameter-Efficient Fine-Tuning (PEFT) (Houlsby et al. 2019) method to reduce the number of trainable parameters, reducing

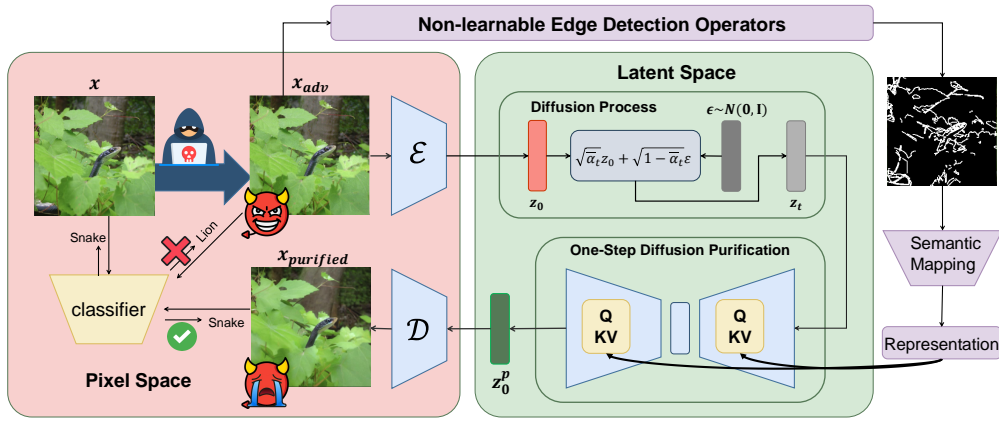


Figure 2: The pipeline of Our proposed One Step Control Purification (OSCP). Our method leverages non-learnable edge detection operators to guide the purification of adversarial samples, avoiding potential inductive bias introduced by neural networks. Our method achieves comparable performance by just running a single step.

the GPU cost and training time when fine-tuning models. ContorlNet (Zhang, Rao, and Agrawala 2023) emerges to provide additional ways to control the generating process, which can use various types of images, such as canny edge, human pose, sketch, and depth map to be the extra image condition for the Stable Diffusion models (SD).

Preliminaries

Diffusion model

Denosing Diffusion Probabilistic Models (DDPM) (Ho, Jain, and Abbeel 2020) generate images by learning from the reverse Markov chain with Gaussian noise added to the original image. The forward process can be formulated as linear combination of original image x_0 and standard Gaussian noise ϵ , $\bar{\alpha}_t$ denoted cumulative product from α_1 to α_t , $\alpha_t = 1 - \beta_t$ for any t , β_t is predefined variance schedule of diffusion process:

$$x_t = \sqrt{\bar{\alpha}_t}x_0 + \sqrt{1 - \bar{\alpha}_t}\epsilon, \epsilon \sim \mathcal{N}(0, \mathbf{I}) \quad (1)$$

and the denoising step can be expressed as:

$$\hat{x}_{t-1} = \frac{1}{\sqrt{\alpha_t}} \left(x_t - \frac{\beta_t}{\sqrt{1 - \bar{\alpha}_t}} \epsilon_{\theta^*}(x_t, t) \right) + \sqrt{\beta_t} \epsilon \quad (2)$$

where model parameter θ^* minimize the loss between actual noise and predict noise:

$$\theta^* = \arg \min_{\theta} \mathbb{E}_{x_0, t, \epsilon} [\|\epsilon - \epsilon_{\theta}(x_t, t)\|_2^2] \quad (3)$$

Shortly, Denosing Diffusion Implicit Models (DDIM) (Song, Meng, and Ermon 2021), a non-Markov inference Process Model, has been invented to reduce the inference time of diffusion model. The denoising step has been respectively modified as:

$$\hat{x}_{t-1} = \sqrt{\bar{\alpha}_{t-1}} \left(\frac{x_t - \sqrt{1 - \bar{\alpha}_t} \epsilon_{\theta^*}(x_t, t)}{\sqrt{\bar{\alpha}_t}} \right) + \sqrt{1 - \bar{\alpha}_{t-1} - \sigma_t^2} \epsilon_{\theta^*}(x_t, t) + \sigma_t \epsilon \quad (4)$$

where $\sigma_t = \eta \cdot \frac{1 - \bar{\alpha}_{t-1}}{1 - \bar{\alpha}_t} \cdot \beta_t$. The denoising process is deterministic if $\eta = 0$ and equals to DDPM if $\eta = 1$.

Diffusion Base Purification (DBP)

DiffPure (Nie et al. 2022) proposes that diffusion models can remove adversarial noise by performing sub-process of the normal reverse process ($t = 0$ to $t = T$). By adding predefined t^* ($t^* < T$) of noise to the adversarial image x_{adv} , which is formed by the sum of original image x and adversarial noise δ , δ can generated by L_p attack (Madry et al. 2018) or AutoAttack (Croce and Hein 2020):

$$\delta = \arg \max_{\delta} \mathcal{L}(C(x + \delta), y) \quad (5)$$

C is the classifier, y is the true label. The forward process of diffusion purification method using:

$$x(t^*) = \sqrt{\bar{\alpha}(t^*)}x + \sqrt{1 - \bar{\alpha}(t^*)}\epsilon \quad (6)$$

and solve the reverse process of DDPM from time step t^* to 0, to get the purified \hat{x}_{adv}^0 that is closed to the original image x , allowing the classifier to classify the image with the correct label.

Consistency function

Diffusion models are known to have long inference time, which limits their usage in real world. Consistency model (Song et al. 2023) has been proposed, aiming the distilled a Consistency model from pretrained diffusion model (CD) or training a Consistency model from scratch (CT), this paper will focus on distilled method. Consistency function can be formulated as:

$$f_{\theta}(x, t) = \begin{cases} x & t = \epsilon \\ F_{\theta}(x, t) & t \in (\epsilon, T] \end{cases} \quad (7)$$

or

$$f_{\theta}(x, t) = c_{\text{skip}}(t)x + c_{\text{out}}(t)F_{\theta}(x, t) \quad (8)$$

where $c_{\text{skip}}(t)$ and $c_{\text{out}}(t)$ are differentiable functions such that $c_{\text{skip}}(\epsilon) = 1$ and $c_{\text{out}}(\epsilon) = 0$.

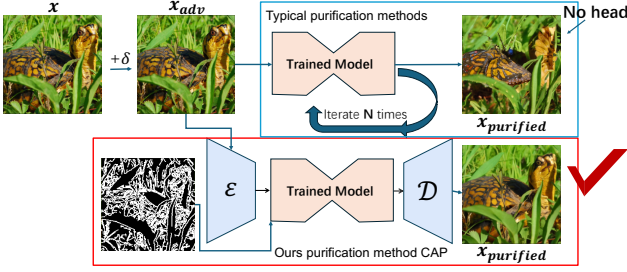


Figure 3: CAP used edge image of the adversarial image to control our purification process, maximizing the remaining semantic information of the purified image.

LCM-LoRA

Due to the efficiency of latent space model compared to pixel-based models, Latent Consistency Model (Luo et al. 2023a) has been proposed, making use of pretrained encoder and decoder to transform images from pixel space to latent space. Latent Consistency Model is parameterized as:

$$f_{\theta}(z, c, t) = c_{\text{skip}}(t)z + c_{\text{out}}(t) \left(\frac{z - \sqrt{1 - \bar{\alpha}_t} \hat{\epsilon}_{\theta}(z, c, t)}{\sqrt{\bar{\alpha}_t}} \right) \quad (9)$$

However, the style LoRAs trained on SDs cannot be used on LCM. Hence, LoRA is introduced to be used on LCM training, the idea of LoRA is separating model parameters into fixed W_0 and low rank matrix decomposition BA , where $B \in \mathbb{R}^{d \times r}$, $A \in \mathbb{R}^{r \times k}$, and the rank $r \leq \min(d, k)$. Training time and computation cost in distillation is reduced by hugely reducing trainable parameters. Also, style LoRA trained on SD can be used on LCM.

Method

In this paper, we aim to solve the slow purification problem in DBP by leveraging the LCM model as the purification backbone, enabling single-step adversarial image purification. However, diffusion models tend to produce images deviating from the originals when purification steps t^* are large (Wang et al. 2022). To address this, we introduce Controlled Adversarial Purification (CAP), shown in Fig. 2, which utilizes ControlNet and edge detection of the original image to guide the purification process.

Furthermore, recognizing that adversarial noise differs from the Gaussian noise that diffusion models are typically designed to remove, we propose Gaussian Adversarial Noise Distillation (GAND). This novel LCM distillation method specifically targets adversarial noise, enhancing the purification performance. Our approach builds upon the insight that combining adversarial purification with adversarial training can yield superior results (Liu et al. 2024), effectively addressing the distinct distributions of Gaussian and adversarial noise.

One Step Control Purification

Problem Definition Our goal can be formulated as:

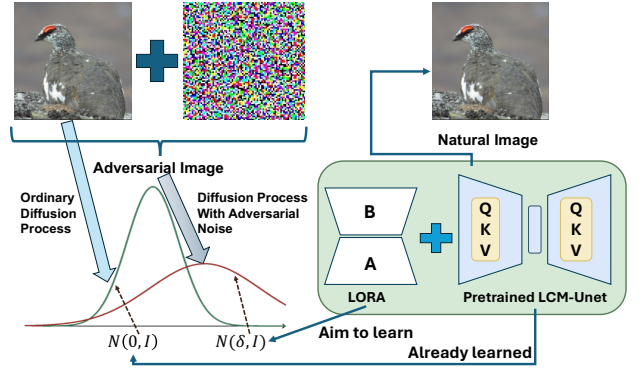


Figure 4: Adversarial images crafted by intentionally attack has shifted distribution after diffusion process differing Standard Normal distribution. GAND tries to learn the additional adversarial noise to recover the attacked images.

$$\begin{aligned} x_{gt} &\simeq \hat{x}_{adv}^0 = \mathcal{D}(f(\mathcal{E}(x_{adv}), t^*)) \\ \text{s.t. } &C(x_{gt}) = C(\hat{x}_{adv}^0) \end{aligned} \quad (10)$$

where x_{gt} is ground truth image, x_{adv} is adversarial image, f is a LCM with the purification function in latent space, t^* is predefined purification step, \mathcal{E} and \mathcal{D} are pretrained image encoder and decoder respectively. For simplifying symbolic, we denote $\mathcal{E}(x_{adv})$ as z_{adv} .

Overview of our method OSCP is illustrated in Fig. 2, OSCP can be separated into two components: a) purification process with nontext guidance and b) training a backbone model with noise and denoise function. We propose Controlled Adversarial Purification (CAP) for a) and Gaussian Adversarial Noise Distillation (GAND), for b).

Controlled Adversarial Purification

To respond to the first component we defined, we propose CAP as Fig. 3, a purification method making use of ControlNet, instead of using image captioning models to generate text prompt guidance, since there exists attack method called Caption semantic attack (Xu et al. 2019), the accuracy of text prompt guidance is generated by those models are questionable. Hence, we prefer to use a traditional and robust method, using an edge detector to get an edge image for guidance.

In purification process, we first encode the adversarial image $z_{adv} = \mathcal{E}(x_{adv})$ to latent space using pre-trained image encoder \mathcal{E} and sample a random noise $\epsilon \sim \mathcal{N}(\mathbf{0}, \mathbf{I})$ in the dimension of the latent space. Then, we diffuse the z_{adv} with predefined strength t^* , using forward latent diffusion process:

$$z_{adv}(t^*) = \sqrt{\bar{\alpha}(t^*)}z_{adv} + \sqrt{1 - \bar{\alpha}(t^*)}\epsilon \quad (11)$$

Then, we purify $z_{adv}(t^*)$ using our LCM trained by GAND, will be discussed in the next subsection, $f_{\theta}(z, c, t)$, z is image latent, c is the condition embedding (e.g., text, canny edge image) and t is time step. The latent consistency function has been introduced in E.q. 9. The purified image latent comes from the latent consistency function, $\hat{z}_{adv}^0 =$

Algorithm 1: GAND

Require: dataset \mathcal{X} , class label of the image \mathbf{y} , classifier C , latent consistency model $f_\theta(\cdot, \cdot, \cdot)$ and its parameter θ , Cross Entropy Loss $L(\cdot, \cdot)$, ODE solver $\Psi(\cdot, \cdot, \cdot, \cdot)$ and distance metric $d(\cdot, \cdot)$. \mathcal{L}_C and \mathcal{L}_G indicate \mathcal{L}_{CIG} (E.q. 18) and \mathcal{L}_{GAND} (E.q. 19) respectively.

- 1: **while** not convergence **do**
- 2: Sample $\mathbf{x} \sim \mathcal{X}$, $n \sim \mathcal{U}[1, (N - k)/2]$
- 3: $\mathbf{z} = \mathcal{E}(\mathbf{x})$
- 4: $\delta_{adv} = \arg \max_\delta L(C(\mathcal{D}(\mathbf{z}) + \delta), \mathbf{y})$ (E.q. 16)
- 5: $\mathbf{z}_{t_{n+k}}^* = \sqrt{\alpha_{t_{n+k}}}\mathbf{z} + \sqrt{1 - \alpha_{t_{n+k}}}(\epsilon + \delta_{adv})$ (E.q. 15)
- 6: $\hat{\mathbf{z}}_{t_n}^\Psi \leftarrow \mathbf{z}_{t_{n+k}}^* + \Psi(\mathbf{z}_{t_{n+k}}^*, t_{n+k}, t_n, \emptyset)$ (E.q. 17)
- 7: $\mathcal{L}_G(\theta, \theta^-) \leftarrow d(f_\theta(\mathbf{z}_{t_{n+k}}^*, \emptyset, t_{n+k}), f_{\theta^-}(\hat{\mathbf{z}}_{t_n}^\Psi, \emptyset, t_n))$
- 8: $\mathcal{L}_C(\theta) \leftarrow d(f_\theta(\mathbf{z}_{t_{n+k}}^*, \emptyset, t_{n+k}), \mathbf{z})$
- 9: $\mathcal{L}_T(\theta, \theta^-) \leftarrow \mathcal{L}_G(\theta, \theta^-) + \lambda_{CIG}\mathcal{L}_C(\theta)$ (E.q. 20)
- 10: $\theta \leftarrow \theta - \eta \nabla_\theta \mathcal{L}(\theta, \theta^-)$
- 11: **end while**

$f_\theta(\mathbf{z}_{adv}(t^*), \mathbf{c}_{ce}, t^*)$, where \mathbf{c}_{ce} means canny edge images which are provided by edge detection operators (Canny 1986), although ControlNet is an extra plug-in tool for Stable Diffusion, \mathbf{c}_{ce} is not exactly an input of f_θ but we treat it as condition embedding here for simplifying the equation. To further reduce the effect of the adversarial image, we remove the $c_{skip}(t)\mathbf{z}_{adv}(t)$ in LCM f_θ and denote this LCM as f_θ^- , since this term will maintain most of the adversarial noise. Therefore, our purified image latent is actually:

$$\begin{aligned} \hat{\mathbf{z}}_{adv}^0 &= f_\theta^-(\mathbf{z}_{adv}(t^*), \mathbf{c}_{ce}, t^*) \\ &= c_{out}(t) \left(\frac{\mathbf{z}_{adv} - \sqrt{1 - \alpha_t} \hat{\epsilon}_\theta(\mathbf{z}_{adv}, \mathbf{c}_{ce}, t)}{\sqrt{\alpha_t}} \right) \end{aligned} \quad (12)$$

Same as setting $c_{skip}(t) \equiv 0$. Finally, We reconstruct the purified image by the image decoder \mathcal{D} , $\hat{\mathbf{x}}_{adv}^0 = \mathcal{D}(\hat{\mathbf{z}}_{adv}^0)$.

Gaussian Adversarial Noise Distillation

To respond to the second component we defined, we propose GAND as Fig. 4, an adversarial distillation framework, which combines adversarial training, Latent Consistency Distillation, and learning how to remove the adversarial and Gaussian noise from the shifted standard Gaussian distribution.

The original LCM distillation first encodes the image to latent code by encoder \mathcal{E} , such that $\mathbf{z} = \mathcal{E}(\mathbf{x})$ and trains the model base on loss function:

$$\begin{aligned} \mathcal{L}(\theta, \theta^-; \Psi) &= \\ &\mathbb{E}_{\mathbf{z}, \mathbf{c}, n} [d(f_\theta(\mathbf{z}_{t_{n+k}}, \mathbf{c}, t_{n+k}), f_{\theta^-}(\hat{\mathbf{z}}_{t_n}^{\Psi, \omega}, \mathbf{c}, t_n))] \end{aligned} \quad (13)$$

where $d(\cdot, \cdot)$ is distance metric, $\Psi(\cdot, \cdot, \cdot, \cdot)$ is DDIM PF-ODE solver Ψ_{DDIM} (Luo et al. 2023a), $f(\cdot, \cdot, \cdot)$ is latent consistency function in E.q. 9 and $\hat{\mathbf{z}}_{t_n}^{\Psi, \omega}$ is an estimation of the solution of the PF-ODE from $t_{n+k} \rightarrow t_n$ using the DDIM PF-ODE solver Ψ :

$$\begin{aligned} \hat{\mathbf{z}}_{t_n}^{\Psi, \omega} &\leftarrow \mathbf{z}_{t_{n+k}} + (1 + \omega)\Psi(\mathbf{z}_{t_{n+k}}, t_{n+k}, t_n, \mathbf{c}) - \\ &\omega\Psi(\mathbf{z}_{t_{n+k}}, t_{n+k}, t_n, \emptyset) \end{aligned} \quad (14)$$

ω is guidance scale and it is sampled from $[\omega_{\min}, \omega_{\max}]$.

We aim to learn the denoise trajectory from a combination of Gaussian noise and adversarial noise to natural image; we need the latent consistency function satisfying that $f_\theta(\mathbf{z}_{adv}(t), \emptyset, t) = f_\theta(\mathbf{z}(t), \emptyset, t) = \mathbf{z}_\epsilon$ for all t . \mathbf{z}_ϵ is the limit of \mathbf{z}_t when $t \rightarrow 0$ where $\mathbf{z}_\epsilon \simeq \mathbf{z}$. However, if we look closely at the definition of consistency function, $f_\theta(\mathbf{z}_{adv}(t), \emptyset, t)$ is converging to \mathbf{z}_{adv} when $t \rightarrow 0$. $f_\theta(\mathbf{z}_{adv}(t), \emptyset, t) - f_\theta(\mathbf{z}(t), \emptyset, t) \rightarrow \delta_{adv}$ when $t \rightarrow 0$, where $\delta_{adv} = \mathbf{z}_{adv} - \mathbf{z}$. Therefore, we introduce \mathbf{z}_t^*

$$\mathbf{z}_t^* = \sqrt{\alpha_t}\mathbf{z} + \sqrt{1 - \alpha_t}(\epsilon + \delta_{adv}) \quad (15)$$

by borrowing the idea of forward diffusion process, making \mathbf{z}_t^* be an linear combination of \mathbf{z} and \mathbf{z}_{adv} , worth to mention that these \mathbf{z}_{adv} used in GAND are generated from latent space attack.

$$\delta_{adv} = \arg \max_\delta \mathcal{L}(C(\mathcal{D}(\mathcal{E}(\mathbf{x}) + \delta)), \mathbf{y}) \quad (16)$$

The $\mathbf{z}_t^* \rightarrow \mathbf{z}$ when $t \rightarrow 0$, and $\mathbf{z}_t^* \rightarrow \epsilon + \delta_{adv}$ when $t \rightarrow T$. Hence, we satisfy the definition of consistency function, which converges to the natural image when t is a small time step and matches with our goal, removing the adversarial noise and Gaussian noise from the shifted normal distribution.

Then, as we do not give condition embeddings, we remove the ω in the formulation of estimation $\hat{\mathbf{z}}_{t_n}^{\Psi, \omega}$ to be:

$$\hat{\mathbf{z}}_{t_n}^\Psi \leftarrow \mathbf{z}_{t_{n+k}} + \Psi(\mathbf{z}_{t_{n+k}}, t_{n+k}, t_n, \emptyset) \quad (17)$$

Where \emptyset means null conditional embedding.

Furthermore, our goal is purifying images instead of image generation, we can train our LCM in a weaker constraint, where we only need the consistency function satisfying on $[0, t]$, $t < T$. Hence, we only simulate the n of time step t_n in $\mathcal{U}[1, (N - k)/2]$. This means that our LCM only satisfies the consistency function on the first half of the time steps.

In addition, we are inspired by (Kim et al. 2024), to add a Clear Image Guide (CIG) loss to further ensure our distillation process is training towards our purification goal. CIG loss is given by:

$$\mathcal{L}_{CIG}(\theta) = \mathbb{E}_{\mathbf{z}, n} [d(f_\theta(\mathbf{z}_{t_{n+k}}^*, \emptyset, t_{n+k}), \mathbf{z})] \quad (18)$$

Therefore, our total distillation loss is the combination of GAND loss

$$\begin{aligned} \mathcal{L}_{GAND}(\theta, \theta^-) &= \\ &\mathbb{E}_{\mathbf{z}, n} [d(f_\theta(\mathbf{z}_{t_{n+k}}^*, \emptyset, t_{n+k}), f_{\theta^-}(\hat{\mathbf{z}}_{t_n}^\Psi, \emptyset, t_n))] \end{aligned} \quad (19)$$

and CIG loss as:

$$\mathcal{L}_{Total}(\theta, \theta^-) = \mathcal{L}_{GAND}(\theta, \theta^-) + \lambda_{CIG}\mathcal{L}_{CIG}(\theta) \quad (20)$$

λ_{CIG} is used to ensure two losses are on the same scale.

The following theorem shows if the loss of GAND converges to an arbitrarily small number, the difference between the purified image and the clean image will be arbitrarily small.

Theorem 1 *If training loss $\mathcal{L}_{Total}(\theta, \theta^-) < \delta$, then we have $\|\mathbf{z} - f_\theta(\mathbf{z}_{adv}(t), \emptyset, t)\| < \mathcal{O}(\delta)$ when t is chosen such that $\alpha_t = 0.5$.*

Proof.

$$\begin{aligned}
& \|z - f_\theta(z_{adv}(t), \emptyset, t)\| \\
& = \|z - f_\theta(z_t^*, \emptyset, t)\| \quad \text{if } \bar{\alpha}_t = 0.5 \\
& = \lambda_{CIG} \mathcal{L}_{CIG}(\theta) / \lambda_{CIG} \\
& \leq \frac{\lambda_{CIG}}{\lambda_{CIG}} \mathcal{L}_{CIG}(\theta) + \frac{\mathcal{L}_{GAND}(\theta, \theta^-)}{\lambda_{CIG}} \quad (21) \\
& = \mathcal{L}_{Total}(\theta, \theta^-) / \lambda_{CIG} \\
& < \mathcal{O}(\delta)
\end{aligned}$$

The first line to second line is true because $z_{adv}(t) - z_t^* = (\sqrt{\bar{\alpha}_t} - \sqrt{1 - \bar{\alpha}_t})\delta_{adv} = 0$ when $\bar{\alpha} = 0.5$.

Experiments and Results

Training setting We distill our adversarial latent consistency model based on SD v1.5 (Rombach et al. 2022), which is trained on resolution 512×512 with ϵ -Prediction (Ho, Jain, and Abbeel 2020). We train our GAND weights with 20,000 iterations with the last 40,000 images from the validation set of ImageNet. The training batch size is 4, with a learning rate of $8e-6$ and a warm-step of 500. For PF-ODE solver Ψ and skipping step k in E.q. 17, we use DDIM-Solver (Song, Meng, and Ermon 2021) with skipping step $k = 20$. Since our training data is not original in the resolution 512×512 , we resize the images to resolution 512×512 ; the adversarial image latent is generated from the clean image latent using PGD-10, with budget 0.03, where the victim model is ResNet50. We set the λ_{CIG} as 0.001. Additionally, our experiment shows that PEFT, i.e., LoRA, is enough.

Attack setting We evaluate our method on the first 10,000 images of validation set ImageNet (Deng et al. 2009), since we use the other 40,000 images of validation set to distillate our model. We consider various architectures, including ResNet50 (He et al. 2016), ResNet152, WideResNet(WRN) (Zagoruyko and Komodakis 2016), and Vision Transformers like ViT-b (Dosovitskiy et al. 2021) and Swin-b (Liu et al. 2021). For attack methods, we consider L_p attacks including PGD (Madry et al. 2018) and AutoAttack (Croce and Hein 2020). For PGD attacks, we use L_∞ norm with bounds $\gamma = 4/255$ and $16/2555$, attack step size $\eta = 1/255$ and $0.025 \cdot 16/255$. For AutoAttack, we use L_∞ norm with $\gamma = 4/255$. In this paper, we denote standard accuracy as testing our framework on clean data, robust accuracy as testing our method on attacked data and clean accuracy as accuracy on clean data of the classifiers without defense. w/o in the tables means no defense is used. PGD- n , n means the number of iterations.

Main Result

We test our model on the 50k ImageNet validation set, which has 1000 classes. Since our method is trained on resolution 512×512 , and does not fit the resolution of classifiers that we use, which are 224. Hence, we resize the image before and after purification step to solve the image size conflict. We take 3 hours for an experiment on an NVIDIA F40 GPU on our method and around 2 days for GDMP (Wang et al. 2022). As shown in Tab. 1, our method outperforms

Defense	Attack Method	Standard	Robust	Architecture
w/o	UT PGD-100	80.55	0.01	ResNet-50
w/o	AutoAttack	80.55	0	ResNet-50
w/o	RT PGD-40	82.33	0.04	ResNet-152
GDMP	UT PGD-100	73.53	72.97	ResNet-50
GDMP	RT PGD-40	78.10	77.86	ResNet-152
DiffPure*	AutoAttack	67.79	40.93	ResNet-50
MS*	AutoAttack	77.96	59.64	ConvNeXt-L
SCH*	AutoAttack	77.00	57.70	ConvNeXt-L
Ours	UT PGD-100	77.63	73.89	ResNet-50
Ours	AutoAttack	77.63	74.19	ResNet-50
Ours	RT PGD-40	79.81	78.78	ResNet-152

Table 1: Accuracy (%) results for ImageNet. The best model is in **bold**. The methods marked with * mean the data are borrowed from the original paper, where SCH refers to the method proposed by Singh, Croce, and Hein (2024); DiffPure refers to that by Nie et al. (2022); MS refers to that by Amini et al. (2024); GDMP refers to that by Wang et al. (2022). UT, RT refers to untargeted, random targeted.

Architecture	Clean	ASR	Standard	Robust
WRN-50-2	82.6	1.0	77.6	75.2
Vit-b-16	81.6	1.0	78.2	71.6
Swin-b	83.6	1.0	79.2	77.8

Table 2: Accuracy (%) and attack success rate (ASR; %) results in various architectures, where the attack method is PGD-100, with budge $4/255$, attack step size $1/255$.

other defense methods, improving robust accuracy 0.92% and 14.55% against PGD-100 ($\gamma = 4/255$) attack and AutoAttack. For random targeted PGD-40 ($\gamma = 16/255$), robust accuracy increases from 77.86% to 78.78%. We choose t^* based on trying strength close to ideal $t^* \approx 350$ from Thm. 1 and we find out that our method performs the best in the step t^* at 200, and this is the purification strength we choose for our method.

Transferability

Our LCM trained by GAND only trains with adversarial images for ResNet50, thus our GAND weight may overfit on those adversarial images. To eliminate this concern, we test our method on three other networks to show the transferability. In Tab. 2, the robust accuracy remains high, where the lowest robust accuracy is 71.6% in ViT $_{b-16}$ model, a vision transformer model. These experiments and the following experiments on ImageNet are run on subset of 500 of the first 10000 images on ImageNet we mentioned before, as we observe that results on subset of 500 and 10000 are similar.

Inference time

One of the goals of our work is to achieve real-time adversarial purification. As shown in Tab. 3, we can see that other diffusion-based purification methods are very time-

Method	Dataset	$t^* \in [0,1000]$	inference time (s)
GDMP	ImageNet	250	~ 9
DiffPure*	ImageNet	150	~ 17
OSCP(Ours)	ImageNet	20/200/500/1000	$\sim \mathbf{0.1}$
OSCP(Ours)	CelabA-HQ	20/200/500/1000	~ 0.5

Table 3: Inference time of purification models to purify a image on an NVIDIA F40 GPU, * means the result is borrowed from the original paper and run on NVIDIA V100 GPU. Notably, GDMP refers to the method proposed by Wang et al. (2022), DiffPure refers to that by Nie et al. (2022).

Defense Method	Arcface	FaceNet	Mobile face
w/o	0.0	0.3	0.0
GaussianBlur ($\sigma = 7.0$)	2.8	51.4	2.8
Das et al. (2018) (n = 60)	17.3	84.1	27.6
CAP(Ours)	83.4	97.8	82.8
OSCP(Ours)	86.8	97.8	84.9

Table 4: Robust accuracy (%) for CelebA-HQ under targeted PGD-10 $L_{\infty\gamma}(\gamma = 4/255)$, $\eta = 0.5*5/255$. The best model is in **bold**.

consuming, and it makes them unsuitable for real-time scenarios. Our method can finish the purification step in 0.1s on ImageNet and 0.5s on CelebA-HQ on any t^* on NVIDIA F40 GPU respectively. Therefore, our method is appropriate for real time cases, e.g., Autonomous Driving.

Face Recognition

We further test our model on a subset of 1000 images on CelebA-HQ dataset (Liu et al. 2015), choosing purification step t^* as 200, control scale 0.8 and borrowing the GAND weight train on ImageNet. We are defending a target PGD attack; the attack is letting Arcface (Deng et al. 2019), FaceNet (Schroff, Kalenichenko, and Philbin 2015), and MobileFaceNet (Chen et al. 2018) recognize any people as a specific person. Our defense goal is to make models not recognize any people as that person, which means the cosine similarity of the embedding of the purified image and the target image is lower than the threshold. Additionally, we show that the GAND weight train on ImageNet is suitable for CelebA-HQ by runing CAP, which is OSCP without GAND in the second last row in Tab. 4. Our GAND weights boost the robust accuracy from 83.4% to 86.8% and 82.8% to 84.9% on Arcface and Mobile face respectively. Also, our methods (CAP and OSCP) have the same robust accuracy 97.8% on FaceNet which is extremely high.

Ablation Studies

We conduct ablations on a subset of 500 images of the validation set on ImageNet, we test CAP on different Controlnet conditioning scale in Fig. 5, and we find out that CAP performs the best at 0.8 conditioning scale. In addition, we demonstrate the effect of CAP and GAND in Tab. 5. When none of our methods are applied (row 1), which means using the original LCM-LoRA, the standard and robust accuracy

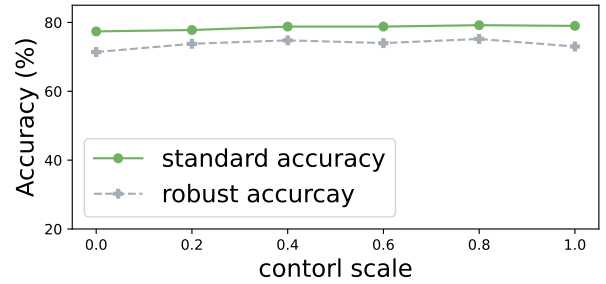


Figure 5: Performance of our method on different t^* under PGD-10 $L_{\infty\gamma}(\gamma = 4/255)$, $\eta = 0.01*4/255$, where we evaluate on ResNet50 on subset of ImageNet validation set.

CAP	GAND	Standard	Robust
X	X	75.0	72.4
X	✓	74.0	72.6
✓	X	77.0	<u>73.2</u>
✓	✓	<u>76.8</u>	75.0

Table 5: Accuracy (%) under PGD-100 $L_{\infty\gamma}(\gamma = 4/255)$, $\eta = 0.01*4/255$. The best performance is in **bold**, and the 2nd best is underlined.

are already high, showing that LCM can be used for adversarial purification. In row 2, we change the LoRA weight from the original LCM-LoRA model to the weight trained by GAND. However, there is only a small increase in robust accuracy. In row 3, we change the purification pipeline to CAP, where a ControlNet is added to the purification framework, using canny edge as control image. The standard and robust accuracy increases 2% and 0.8% respectively. Finally, we combine two methods, forming our OSCP (row 4), hugely increase the robust accuracy from 72.4% in row 1 to 75% in row 4. These results illustrate the robust performance of our methods.

Discussion and Conclusion

In this work, we propose OSCP, an edge image controlled adversarial purification, combining with adversarial trained LCM-LoRA, which is trained by GAND, achieving superior efficiency. However, the purification step is still found by trial and error which is time consuming, this is another long-standing problem, finding adaptive purification strength might be a future breakthrough in diffusion-based purification methods. In summary, our contribution includes finding a rapid purification method and a novel controlled adversarial purification framework.

References

Amini, S.; Teymoorianfard, M.; Ma, S.; and Houmansadr, A. 2024. MeanSparse: Post-Training Robustness Enhancement Through Mean-Centered Feature Sparsification. *arXiv preprint arXiv:2406.05927*.

- Athalye, A.; Carlini, N.; and Wagner, D. 2018. Obfuscated gradients give a false sense of security: Circumventing defenses to adversarial examples. In *International Conference on Machine Learning*, 274–283. PMLR.
- Blattmann, A.; Rombach, R.; Ling, H.; Dockhorn, T.; Kim, S. W.; Fidler, S.; and Kreis, K. 2023. Align Your Latents: High-Resolution Video Synthesis With Latent Diffusion Models. In *Proceedings of the IEEE/CVF Conference on Computer Vision and Pattern Recognition (CVPR)*, 22563–22575.
- Canny, J. 1986. A computational approach to edge detection. *IEEE Transactions on Pattern Analysis and Machine Intelligence*, PAMI-8(6): 679–698.
- Chen, S.; Liu, Y.; Gao, X.; and Han, Z. 2018. MobileFaceNets: Efficient CNNs for Accurate Real-Time Face Verification on Mobile Devices. In *Biometric Recognition*, 428–438. Springer International Publishing. ISBN 978-3-319-97909-0.
- Croce, F.; and Hein, M. 2020. Reliable evaluation of adversarial robustness with an ensemble of diverse parameter-free attacks. In *International Conference on Machine Learning*, 2206–2216. PMLR.
- Das, N.; Shanbhogue, M.; Chen, S.-T.; Hohman, F.; Li, S.; Chen, L.; Kounavis, M. E.; and Chau, D. H. 2018. Shield: Fast, practical defense and vaccination for deep learning using jpeg compression. In *Proceedings of the 24th ACM SIGKDD International Conference on Knowledge Discovery & Data Mining*, 196–204.
- Deng, J.; Dong, W.; Socher, R.; Li, L.-J.; Li, K.; and Fei-Fei, L. 2009. Imagenet: A large-scale hierarchical image database. In *2009 IEEE Conference on Computer Vision and Pattern Recognition*, 248–255. IEEE.
- Deng, J.; Guo, J.; Xue, N.; and Zafeiriou, S. 2019. ArcFace: Additive Angular Margin Loss for Deep Face Recognition. In *Proceedings of the IEEE/CVF Conference on Computer Vision and Pattern Recognition (CVPR)*.
- Dosovitskiy, A.; Beyer, L.; Kolesnikov, A.; Weissenborn, D.; Zhai, X.; Unterthiner, T.; Dehghani, M.; Minderer, M.; Heigold, G.; Gelly, S.; Uszkoreit, J.; and Houlsby, N. 2021. An Image is Worth 16x16 Words: Transformers for Image Recognition at Scale. In *International Conference on Learning Representations*.
- Girshick, R.; Donahue, J.; Darrell, T.; and Malik, J. 2014. Rich Feature Hierarchies for Accurate Object Detection and Semantic Segmentation. In *Proceedings of the IEEE Conference on Computer Vision and Pattern Recognition (CVPR)*.
- Gowal, S.; Qin, C.; Uesato, J.; Mann, T.; and Kohli, P. 2020. Uncovering the Limits of Adversarial Training against Norm-Bounded Adversarial Examples. *arXiv e-prints*, arXiv:2010.
- Gowal, S.; Rebuffi, S.-A.; Wiles, O.; Stimberg, F.; Calian, D. A.; and Mann, T. A. 2021. Improving robustness using generated data. *Advances in Neural Information Processing Systems*, 34: 4218–4233.
- Guo, Z.; Wang, K.; Li, W.; Qian, Y.; Arandjelović, O.; and Fang, L. 2024. Artwork protection against neural style transfer using locally adaptive adversarial color attack. *arXiv preprint arXiv:2401.09673*.
- He, K.; Zhang, X.; Ren, S.; and Sun, J. 2016. Deep Residual Learning for Image Recognition. In *Proceedings of the IEEE Conference on Computer Vision and Pattern Recognition (CVPR)*.
- Ho, J.; Jain, A.; and Abbeel, P. 2020. Denoising diffusion probabilistic models. *Advances in Neural Information Processing Systems*, 33: 6840–6851.
- Ho, J.; Salimans, T.; Gritsenko, A.; Chan, W.; Norouzi, M.; and Fleet, D. J. 2022. Video diffusion models. *Advances in Neural Information Processing Systems*, 35: 8633–8646.
- Houlsby, N.; Giurgiu, A.; Jastrzebski, S.; Morrone, B.; De Laroussilhe, Q.; Gesmundo, A.; Attariyan, M.; and Gelly, S. 2019. Parameter-efficient transfer learning for NLP. In *International Conference on Machine Learning*, 2790–2799. PMLR.
- Huang, S.; Kathirvel, R. P.; Lau, C. P.; and Chellappa, R. 2023. Whole-body detection, recognition and identification at altitude and range. *arXiv preprint arXiv:2311.05725*.
- Kim, D.; Lai, C.-H.; Liao, W.-H.; Murata, N.; Takida, Y.; Uesaka, T.; He, Y.; Mitsufuji, Y.; and Ermon, S. 2024. Consistency Trajectory Models: Learning Probability Flow ODE Trajectory of Diffusion. In *International Conference on Learning Representations*.
- Krizhevsky, A.; Sutskever, I.; and Hinton, G. E. 2012. Imagenet classification with deep convolutional neural networks. *Advances in Neural Information Processing Systems*, 25.
- Lau, C. P.; Liu, J.; Lin, W.-A.; Souri, H.; Khorramshahi, P.; and Chellappa, R. 2023a. Adversarial attacks and robust defenses in deep learning. In *Handbook of Statistics*, volume 48, 29–58. Elsevier.
- Lau, C. P.; Liu, J.; Souri, H.; Lin, W.-A.; Feizi, S.; and Chellappa, R. 2023b. Interpolated joint space adversarial training for robust and generalizable defenses. *IEEE Transactions on Pattern Analysis and Machine Intelligence*, 45(11): 13054–13067.
- Lin, W.-A.; Lau, C. P.; Levine, A.; Chellappa, R.; and Feizi, S. 2020. Dual Manifold Adversarial Robustness: Defense against Lp and non-Lp Adversarial Attacks. In *Advances in Neural Information Processing Systems*, volume 33, 3487–3498.
- Liu, F.; Chen, D.; Wang, F.; Li, Z.; and Xu, F. 2023a. Deep learning based single sample face recognition: a survey. *Artificial Intelligence Review*, 56(3): 2723–2748.
- Liu, J.; Lau, C. P.; and Chellappa, R. 2023. Diffprotect: Generate adversarial examples with diffusion models for facial privacy protection. *arXiv preprint arXiv:2305.13625*.
- Liu, J.; Lau, C. P.; Souri, H.; Feizi, S.; and Chellappa, R. 2022a. Mutual adversarial training: Learning together is better than going alone. *IEEE Transactions on Information Forensics and Security*, 17: 2364–2377.
- Liu, J.; Levine, A.; Lau, C. P.; Chellappa, R.; and Feizi, S. 2022b. Segment and Complete: Defending Object Detectors Against Adversarial Patch Attacks With Robust Patch

- Detection. In *Proceedings of the IEEE/CVF Conference on Computer Vision and Pattern Recognition (CVPR)*, 14973–14982.
- Liu, J.; Wei, C.; Guo, Y.; Yu, H.; Yuille, A.; Feizi, S.; Lau, C. P.; and Chellappa, R. 2023b. Instruct2Attack: Language-Guided Semantic Adversarial Attacks. *arXiv preprint arXiv:2311.15551*.
- Liu, Y.; Liu, K.; Xiao, Y.; Dong, Z.; Xu, X.; Wei, P.; and Lin, L. 2024. Towards Better Adversarial Purification via Adversarial Denoising Diffusion Training. *arXiv preprint arXiv:2404.14309*.
- Liu, Z.; Lin, Y.; Cao, Y.; Hu, H.; Wei, Y.; Zhang, Z.; Lin, S.; and Guo, B. 2021. Swin Transformer: Hierarchical Vision Transformer Using Shifted Windows. In *Proceedings of the IEEE/CVF International Conference on Computer Vision (ICCV)*, 10012–10022.
- Liu, Z.; Luo, P.; Wang, X.; and Tang, X. 2015. Deep Learning Face Attributes in the Wild. In *Proceedings of the IEEE International Conference on Computer Vision (ICCV)*.
- Luo, S.; and Hu, W. 2021. Diffusion Probabilistic Models for 3D Point Cloud Generation. In *Proceedings of the IEEE/CVF Conference on Computer Vision and Pattern Recognition (CVPR)*, 2837–2845.
- Luo, S.; Tan, Y.; Huang, L.; Li, J.; and Zhao, H. 2023a. Latent Consistency Models: Synthesizing High-Resolution Images with Few-Step Inference. *arXiv e-prints*, arXiv–2310.
- Luo, S.; Tan, Y.; Patil, S.; Gu, D.; von Platen, P.; Passos, A.; Huang, L.; Li, J.; and Zhao, H. 2023b. LCM-LoRA: A Universal Stable-Diffusion Acceleration Module. *arXiv e-prints*, arXiv–2311.
- Madry, A.; Makelov, A.; Schmidt, L.; Tsipras, D.; and Vladu, A. 2018. Towards Deep Learning Models Resistant to Adversarial Attacks. In *International Conference on Learning Representations*.
- Minaee, S.; Boykov, Y.; Porikli, F.; Plaza, A.; Kehtarnavaz, N.; and Terzopoulos, D. 2021. Image segmentation using deep learning: A survey. *IEEE Transactions on Pattern Analysis and Machine Intelligence*, 44(7): 3523–3542.
- Nie, W.; Guo, B.; Huang, Y.; Xiao, C.; Vahdat, A.; and Anandkumar, A. 2022. Diffusion Models for Adversarial Purification. In *International Conference on Machine Learning*, 16805–16827. PMLR.
- Paszke, A.; Gross, S.; Massa, F.; Lerer, A.; Bradbury, J.; Chanan, G.; Killeen, T.; Lin, Z.; Gimelshein, N.; Antiga, L.; et al. 2019. Pytorch: An imperative style, high-performance deep learning library. *Advances in Neural Information Processing Systems*, 32.
- Picard, D. 2021. Torch. manual_seed (3407) is all you need: On the influence of random seeds in deep learning architectures for computer vision. *arXiv preprint arXiv:2109.08203*.
- Poole, B.; Jain, A.; Barron, J. T.; and Mildenhall, B. 2023. DreamFusion: Text-to-3D using 2D Diffusion. In *International Conference on Learning Representations*.
- Rebuffi, S.-A.; Goyal, S.; Calian, D. A.; Stimberg, F.; Wiles, O.; and Mann, T. 2021. Fixing Data Augmentation to Improve Adversarial Robustness. *arXiv e-prints*, arXiv–2103.
- Rombach, R.; Blattmann, A.; Lorenz, D.; Esser, P.; and Ommer, B. 2022. High-Resolution Image Synthesis with Latent Diffusion Models. In *2022 IEEE/CVF Conference on Computer Vision and Pattern Recognition (CVPR)*, 10674–10685. IEEE.
- Saharia, C.; Chan, W.; Saxena, S.; Li, L.; Whang, J.; Denton, E. L.; Ghasemipour, K.; Gontijo Lopes, R.; Karagol Ayan, B.; Salimans, T.; et al. 2022. Photorealistic text-to-image diffusion models with deep language understanding. *Advances in Neural Information Processing Systems*, 35: 36479–36494.
- Samangouei, P.; Kabkab, M.; and Chellappa, R. 2018. Defense-GAN: Protecting Classifiers Against Adversarial Attacks Using Generative Models. In *International Conference on Learning Representations*.
- Schroff, F.; Kalenichenko, D.; and Philbin, J. 2015. FaceNet: A Unified Embedding for Face Recognition and Clustering. In *Proceedings of the IEEE Conference on Computer Vision and Pattern Recognition (CVPR)*.
- Simonyan, K.; and Zisserman, A. 2015a. Very Deep Convolutional Networks for Large-Scale Image Recognition. In *International Conference on Learning Representations*. Computational and Biological Learning Society.
- Simonyan, K.; and Zisserman, A. 2015b. Very Deep Convolutional Networks for Large-Scale Image Recognition. In *International Conference on Learning Representations*.
- Singh, N. D.; Croce, F.; and Hein, M. 2024. Revisiting adversarial training for imagenet: Architectures, training and generalization across threat models. *Advances in Neural Information Processing Systems*, 36.
- Song, J.; Meng, C.; and Ermon, S. 2021. Denoising Diffusion Implicit Models. In *International Conference on Learning Representations*.
- Song, Y.; Dhariwal, P.; Chen, M.; and Sutskever, I. 2023. Consistency Models. In *International Conference on Machine Learning*, 32211–32252. PMLR.
- Song, Y.; and Ermon, S. 2019. Generative modeling by estimating gradients of the data distribution. *Advances in Neural Information Processing Systems*, 32.
- Souri, H.; Khorramshahi, P.; Lau, C. P.; Goldblum, M.; and Chellappa, R. 2021. Identification of attack-specific signatures in adversarial examples. *arXiv preprint arXiv:2110.06802*.
- Tramer, F.; and Boneh, D. 2019. Adversarial training and robustness for multiple perturbations. *Advances in Neural Information Processing Systems*, 32.
- von Platen, P.; Patil, S.; Lozhkov, A.; Cuenca, P.; Lambert, N.; Rasul, K.; Davaadorj, M.; Nair, D.; Paul, S.; Berman, W.; Xu, Y.; Liu, S.; and Wolf, T. 2022. Diffusers: State-of-the-art diffusion models. <https://github.com/huggingface/diffusers>.
- Wang, J.; Lyu, Z.; Lin, D.; Dai, B.; and Fu, H. 2022. Guided diffusion model for adversarial purification. *arXiv preprint arXiv:2205.14969*.
- Wang, Z.; Bovik, A. C.; Sheikh, H. R.; and Simoncelli, E. P. 2004. Image quality assessment: from error visibility to structural similarity. *IEEE Transactions on Image Processing*, 13(4): 600–612.

Wang, Z.; Pang, T.; Du, C.; Lin, M.; Liu, W.; and Yan, S. 2023. Better diffusion models further improve adversarial training. In *International Conference on Machine Learning*, 36246–36263. PMLR.

Xu, Y.; Wu, B.; Shen, F.; Fan, Y.; Zhang, Y.; Shen, H. T.; and Liu, W. 2019. Exact Adversarial Attack to Image Captioning via Structured Output Learning With Latent Variables. In *Proceedings of the IEEE/CVF Conference on Computer Vision and Pattern Recognition (CVPR)*.

Xue, H.; Araujo, A.; Hu, B.; and Chen, Y. 2024. Diffusion-based adversarial sample generation for improved stealthiness and controllability. *Advances in Neural Information Processing Systems*, 36.

Yoon, J.; Hwang, S. J.; and Lee, J. 2021. Adversarial purification with score-based generative models. In *International Conference on Machine Learning*, 12062–12072. PMLR.

Yue, Y.; and Li, Z. 2024. Medmamba: Vision mamba for medical image classification. *arXiv preprint arXiv:2403.03849*.

Zagoruyko, S.; and Komodakis, N. 2016. Wide Residual Networks. In *British Machine Vision Conference 2016*. British Machine Vision Association.

Zhang, L.; Rao, A.; and Agrawala, M. 2023. Adding Conditional Control to Text-to-Image Diffusion Models. In *Proceedings of the IEEE/CVF International Conference on Computer Vision (ICCV)*, 3836–3847.

Zhang, R.; Isola, P.; Efros, A. A.; Shechtman, E.; and Wang, O. 2018. The Unreasonable Effectiveness of Deep Features as a Perceptual Metric. In *Proceedings of the IEEE Conference on Computer Vision and Pattern Recognition (CVPR)*.

Zhao, Z.-Q.; Zheng, P.; Xu, S.-t.; and Wu, X. 2019. Object detection with deep learning: A review. *IEEE Transactions on Neural Networks and Learning Systems*, 30(11): 3212–3232.

Zheng, J.; Hu, M.; Fan, Z.; Wang, C.; Ding, C.; Tao, D.; and Cham, T.-J. 2024. Trajectory consistency distillation. *arXiv preprint arXiv:2402.19159*.

Appendix

Additional implementation details

We implement our method with Pytorch (Paszke et al. 2019) and Diffusers (von Platen et al. 2022). we fix the random seed of PyTorch’s generator as 100 for the reproducibility (Picard 2021).

For all implementation, we use the same version of AutoAttack, which is same in both main paper and the appendix.

We leverage LCM-LoRA¹ (Luo et al. 2023b) and TCD-LoRA² (Zheng et al. 2024) from their HuggingFace repositories.

In terms of training with our proposed GAND, we use the Stable Diffusion v1.5³ (SD15) as the teacher model.

We borrow a part of code and pretrained weights from AMT-GAN⁴ when we do experiments on CelebA-HQ.

Unless mentioned, all reproducibility-related things follows the above.

Edge detector

For someone who may be concerned, edge detectors usually consider high-frequency pixels as edges; then, if we use those edge images for ControlNet, OSCP will reserve those high-frequency pixels in the purified image. To avoid this problem, we extra blur the images before they are inserted into the edge detector. In Fig. 6, the edge image on the right side, conducted by an adversarial image without blur, is full of noise. Meanwhile, the edge image in the middle is connected by the adversarial image with extra blur, which has most of the contour of the clean image on the left side.



Figure 6: The left side is clean image. The middle is canny edge image with extra blur. The right side is canny edge image without extra blur

Proofs

We are going to provide some simple proofs for things we have claimed, including

1. $z_t^* \rightarrow z$ when $t \rightarrow 0$,
2. $z_t^* \rightarrow \epsilon + \delta_{adv}$ when $t \rightarrow T$
3. $f_\theta(z_{adv}(t), \emptyset, t) \rightarrow z_{adv}$ when $t \rightarrow 0$
4. $f_\theta(z_{adv}(t), \emptyset, t) - f_\theta(z(t), \emptyset, t) \rightarrow \delta_{adv}$ when $t \rightarrow 0$

Lemma. If $X \sim \mathcal{N}(\mu, \sigma^2)$ and $\sigma^2 \rightarrow 0$, then $X \rightarrow \mu$

Proof. For any $\epsilon > 0$,

$$\begin{aligned} P(\|X - \mu\| \geq \epsilon) &= P(\|Z\| \geq \epsilon) \quad Z \sim \mathcal{N}(0, \sigma^2) \\ &\leq \frac{E(X^2)}{\epsilon^2} \quad \text{Markov's inequality} \\ &= \frac{\text{Var}(X) + (E(X))^2}{\epsilon^2} = \frac{\sigma^2}{\epsilon^2} \rightarrow 0 \end{aligned} \tag{22}$$

¹<https://huggingface.co/latent-consistency/lcm-lora-sdv1-5>

²<https://huggingface.co/h1t/TCD-SD15-LoRA>

³<https://huggingface.co/runwayml/stable-diffusion-v1-5>

⁴<https://github.com/CGCL-codes/AMT-GAN>

Proof 1. β_t is increasing sequence in $t \in \{0, 1, \dots, T-1, T\}$ in range $(0, 1)$, then we have $\alpha_t = 1 - \beta_t$ is decreasing sequence in $t \in \{0, 1, \dots, T-1, T\}$ in range $(0, 1)$, $\bar{\alpha}_t$ is decreasing step function in range $(0, 1)$, further assume β_0 is a arbitrarily small number:

$$\begin{aligned} \lim_{t \rightarrow 0} \mathbf{z}_t^* &= \lim_{t \rightarrow 0} \sqrt{\bar{\alpha}_t} \mathbf{z} + \sqrt{1 - \bar{\alpha}_t} (\boldsymbol{\epsilon} + \boldsymbol{\delta}_{adv}) \\ &= \sqrt{\alpha_0} \mathbf{z} + \sqrt{1 - \alpha_0} (\boldsymbol{\epsilon} + \boldsymbol{\delta}_{adv}) \\ &= \sqrt{1 - \beta_0} \mathbf{z} + \sqrt{\beta_0} \boldsymbol{\epsilon} + \sqrt{\beta_0} \boldsymbol{\delta}_{adv} \\ &= \mathbf{z} + \sqrt{\beta_0} \boldsymbol{\epsilon} \quad \text{by assumption on } \beta_0 \end{aligned} \quad (23)$$

since we know $\mathbf{z} + \sqrt{\beta_0} \boldsymbol{\epsilon} \sim \mathcal{N}(\mathbf{z}, \beta_0 \mathbf{I})$ and β_0 is vanishing. By lemma, we have $\mathbf{z}_t^* \rightarrow \mathbf{z}$.

Proof 2. β_t is increasing sequence in $t \in \{0, 1, \dots, T-1, T\}$ in range $(0, 1)$, then we have α_t is decreasing sequence in $t \in \{0, 1, \dots, T-1, T\}$ in range $(0, 1)$, $\bar{\alpha}_t$ is decreasing step function in range $(0, 1)$, further assume T is a arbitrarily large number, consider $\boldsymbol{\delta}_{adv}$ as constant.

$$\begin{aligned} \bar{\alpha}_T &= \prod_{t=0}^T \alpha_t = \prod_{t=0}^T (1 - \beta_t) \leq (1 - \beta_0)^{T+1} \rightarrow 0 \quad \text{by assuming } T \text{ is arbitrarily large} \\ \lim_{t \rightarrow T} \mathbf{z}_t^* &= \lim_{t \rightarrow T} \sqrt{\bar{\alpha}_t} \mathbf{z} + \sqrt{1 - \bar{\alpha}_t} (\boldsymbol{\epsilon} + \boldsymbol{\delta}_{adv}) \\ &= \boldsymbol{\epsilon} + \boldsymbol{\delta}_{adv} \sim \mathcal{N}(\boldsymbol{\delta}_{adv}, \mathbf{I}) \end{aligned} \quad (24)$$

Proof 3. β_t is increasing sequence in $t \in \{0, 1, \dots, T-1, T\}$ in range $(0, 1)$, then we have α_t is linear decreasing sequence in $t \in \{0, 1, \dots, T-1, T\}$ in range $(0, 1)$, $\bar{\alpha}_t$ is decreasing step function in range $(0, 1)$, further assume $\hat{\boldsymbol{\epsilon}}$ has standard Gaussian distribution and β_0 is a arbitrarily small number.

$$\begin{aligned} \lim_{t \rightarrow 0} f_\theta(\mathbf{z}_{adv}(t), \emptyset, t) &= \lim_{t \rightarrow 0} \frac{\sigma^2}{t^2 + \sigma^2} \mathbf{z}_{adv}(t) + \frac{t^2}{\sqrt{t^2 + \sigma^2}} \left(\frac{\mathbf{z}_{adv}(t) - \sqrt{1 - \bar{\alpha}_t} \hat{\boldsymbol{\epsilon}}(\mathbf{z}_{adv}(t), \mathbf{c}, t)}{\sqrt{\bar{\alpha}_t}} \right) \\ &= \lim_{t \rightarrow 0} \frac{\sigma^2}{t^2 + \sigma^2} \mathbf{z}_{adv}(t) + \lim_{t \rightarrow 0} \frac{t^2}{\sqrt{t^2 + \sigma^2}} \left(\frac{\mathbf{z}_{adv}(t) - \sqrt{1 - \bar{\alpha}_t} \hat{\boldsymbol{\epsilon}}}{\sqrt{\bar{\alpha}_t}} \right) \\ &= \lim_{t \rightarrow 0} \sqrt{\bar{\alpha}_t} \mathbf{z}_{adv} + \sqrt{1 - \bar{\alpha}_t} \boldsymbol{\epsilon} - \lim_{t \rightarrow 0} \frac{t^2}{\sqrt{t^2 + \sigma^2}} \left(\frac{\sqrt{1 - \bar{\alpha}_t} \hat{\boldsymbol{\epsilon}}}{\sqrt{\bar{\alpha}_t}} \right) \\ &= \sqrt{\alpha_0} \mathbf{z}_{adv} + \sqrt{1 - \alpha_0} \boldsymbol{\epsilon} - \lim_{t \rightarrow 0} \frac{t^2}{\sqrt{t^2 + \sigma^2}} \left(\frac{\sqrt{1 - \alpha_0} \hat{\boldsymbol{\epsilon}}}{\sqrt{\alpha_0}} \right) \\ &= \mathbf{z}_{adv} + \sqrt{\beta_0} \boldsymbol{\epsilon} - \lim_{t \rightarrow 0} \frac{t^2}{\sqrt{t^2 + \sigma^2}} \left(\sqrt{\beta_0} \right) \hat{\boldsymbol{\epsilon}} \quad \text{by assumption on } \beta_0 \\ &= \mathbf{z}_{adv} + \lim_{t \rightarrow 0} \sqrt{\left(1 + \frac{t^4}{t^2 + \sigma^2} \right)} \beta_0 \boldsymbol{\epsilon} \quad \text{by the property of normal distribution and assumption on } \hat{\boldsymbol{\epsilon}} \end{aligned} \quad (25)$$

By $\lim_{t \rightarrow 0} \sqrt{\left(1 + \frac{t^4}{t^2 + \sigma^2} \right)} = 0$ and lemma we have proved, $f_\theta(\mathbf{z}_{adv}(t), \emptyset, t) \rightarrow \mathbf{z}_{adv}$.

Proof 4. Following the proof 3, we have

$$\begin{aligned} \lim_{t \rightarrow 0} f_\theta(\mathbf{z}(t), \emptyset, t) &= \mathbf{z} + \lim_{t \rightarrow 0} \sqrt{\left(1 + \frac{t^4}{t^2 + \sigma^2} \right)} \beta_0 \boldsymbol{\epsilon} \\ \lim_{t \rightarrow 0} f_\theta(\mathbf{z}_{adv}(t), \emptyset, t) - f_\theta(\mathbf{z}(t), \emptyset, t) &= \mathbf{z}_{adv} - \mathbf{z} + \lim_{t \rightarrow 0} \sqrt{2 \left(1 + \frac{t^4}{t^2 + \sigma^2} \right)} \beta_0 \boldsymbol{\epsilon} \\ &\rightarrow \mathbf{z}_{adv} - \mathbf{z} = \boldsymbol{\delta}_{adv} \quad \text{same as proof 3 and by the definition of } \boldsymbol{\delta}_{adv} \end{aligned} \quad (26)$$

Experiment

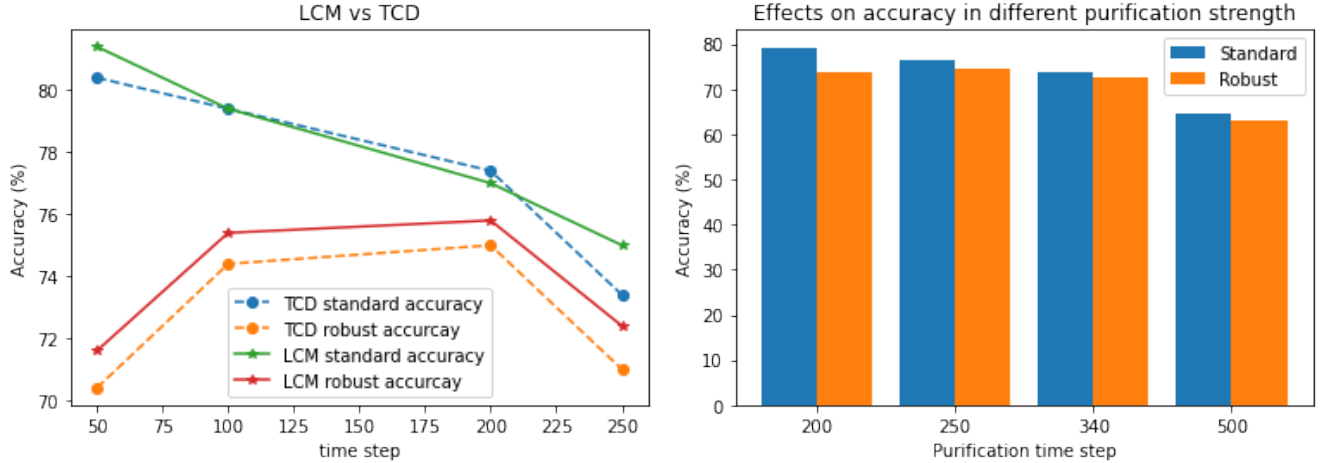


Figure 7: a) Accuracy (%) using LCM and TCD model as defense model. b) Accuracy (%) on different purification time step t^* on our method. Two figures have the same attack setting, PGD-100 $L_{\infty}\gamma$ ($\gamma = 4/255$), step size $0.01 * 4/255$, where both we evaluate on ResNet50 on 500 subset of ImageNet validation set.

In Fig. 7a), we test the robustness of another model, Trajectory consistency distillation (TCD) (Zheng et al. 2024), which can also generate an image in one step. We can see that using LCM as purification model is generally more robust than using TCD. Also, the standard accuracy of two models are similar. Therefore, we choose LCM as our backbone model for purification instead of TCD.

In Fig. 7b), we show the experiment for choosing purification time step on ImageNet. We can see the robust accuracy of the $t^* = 340$, which is close to the ideal t^* from thm. 1 in main paper, is already very high. However, the performance is the best at $t^* = 200$ in both standard accuracy and robust accuracy. Hence, we decide to choose $t^* = 200$ for our method on ImageNet.

$c_{skip}(t)z_t$	Accuracy (%)	$t^* = 20$	$t^* = 60$	$t^* = 100$	$t^* = 200$	$t^* = 250$
\times	Robust	43.4	56.0	59.4	66.4	68.4
\times	Standard	81.2	81.4	81.2	79.2	76.6
\checkmark	Robust	44.2	54.8	60.4	66.0	67.8
\checkmark	Standard	81.2	81.4	81.2	79.2	76.6

Table 6: Accuracy with and without $c_{skip}(t)z_t$ term in LCM in our method under PGD-10 ($\gamma = 8/255$), $\eta = 2/255$ on ResNet50 on a subset of 500 images ImageNet validation set.

In Tab. 6, we conduct ablations on E.q. 12 in the main paper, and we can see that the standard accuracy does not change with or without the term $c_{skip}(t)z_t$. However, the robust accuracy is higher on average if we take away the term $c_{skip}(t)z_t$ from LCM. This is because z_t is from the original input image without denoise, and remains the adversarial noise if input is adversarial image. Therefore, we have decided to remove this term from LCM.

Accuracy (%)	$\frac{N-k}{4}$	$\frac{N-k}{2}$	$\frac{3(N-k)}{4}$	$N - k$
Robust	74.0	74.3	73.7	73.6
Standard	78.8	79.4	79.1	79.1

Table 7: Accuracy of our method under AutoAttack ($\gamma = 8/255$) on ResNet50 on a subset of 1000 images ImageNet validation set on different set of training time step. ($t^* = 200$)

In Tab. 7, we further test three more different sets of training time steps, since we mentioned in main paper, our goal is purification not generation, we can set a smaller training time step set for GAND. We sample subscript n of t_n in $\mathcal{U}[1, (N-k)/4]$,

$\mathcal{U}[1, (N - k)/2]$, $\mathcal{U}[1, 3(N - k)/4]$ and $\mathcal{U}[1, N - k]$ (original case) respectively, other settings are same as the training recipe we describe in Experiment section. As shown in Tab. 7, the standard and robust accuracy decrease if we sample the training time step in a larger set. Therefore, we can conclude that if our goal is purification, we can just fine-tune LCM in small time steps.

Method	Resolution	$t^* = 20$	$t^* = 60$	$t^* = 100$	$t^* = 250$	$t^* = 500$
DiffPure	256×256	~ 0.5	~ 0.7	~ 1	~ 2	~ 3.5
DiffPure	512×512	~ 1.5	~ 2.5	~ 3.5	~ 7.5	~ 14
DiffPure	1024×1024	~ 5	~ 10	~ 14	~ 30	~ 60
Ours	256×256	~ 0.05	~ 0.05	~ 0.05	~ 0.05	~ 0.05
Ours	512×512	~ 0.08	~ 0.08	~ 0.08	~ 0.08	~ 0.08
Ours	1024×1024	~ 0.1	~ 0.1	~ 0.1	~ 0.1	~ 0.1

Table 8: Inference time (s) of of our method on different inference time and resolution

In Tab. 8, we further test the inference time of our method on three resolutions without resizing on an NVIDIA F40 GPU. This result showcases that if GAND weights are trained on those resolutions, what will the inference time of our method be. We reproduce DiffPure (Nie et al. 2022) by using DDIM-50 as purification model in this experiment. As shown in Tab. 8, DiffPure, using DDIM-50, takes around a minute to purify a 1024×1024 image when t^* is chosen to be 500. Meanwhile, our method only takes 0.1 seconds to purify a 1024×1024 image on any t^* , showing the potential of our method for purification in high-resolution images. DDIM-50 denotes skipping step k of DDIM is set as 20.

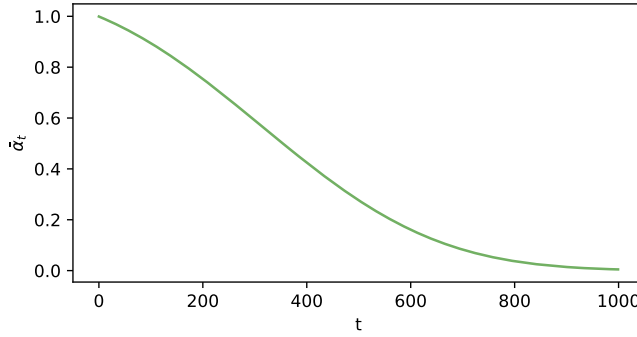


Figure 8: Visualization of how the term $\bar{\alpha}_t$ change by t

In Fig. 8, we show how $\bar{\alpha}_t$ variate by t in the LCM scheduler⁵. We can see that $\bar{\alpha}_t = 0.5$ when $t \approx 350$. The value of $\bar{\alpha}_t$ start at almost 1 ($t = 0$) and decrease to almost 0 ($t = 1000$), which meet with the assumptions we have made in our proofs.

Defence method	ResNet-50	ResNet-152	WideResNet-50-2	Vit-b-16	Swin-b	ConvNeXt-b
DiffPure ($t^* = 100$)	53.8	49.4	52.2	16.6	45.1	42.9
Ours ($t^*=250$)	59.0	56.5	57.9	34.1	53.9	49.1

Table 9: Robust Accuracy (%) on our method under Diff-PGD-10 attack $\gamma = 8/255$ ($\eta = 2/255$) on a subset of 1000 images ImageNet validation set

In Tab. 9, we test our method under version 2 of Diff-PGD attack (Xue et al. 2024), which is a SOTA attack method. We use DDIM as the backbone model of DiffPure. In Tab. 9, our method boost the robust accuracy in Vit-b-16 from 16.6% to 34.1%. In ResNet-50, ResNet-152, WideResNet-50-2, the robust accuracy increase 5.2%, 7.1% and 5.7% respectively. For robust accuracy in Swin-b and ConvNeXt, our method acheive 53.9% and 49.1%, which is 8.8% and 6.2% higher than DiffPure.

Although our goal is purification, it is still interesting for us to visualize the image generated by our GAND weight. We use LCM-LoRA¹ and change their LoRA to our GAND LoRA weight. Then, we generate pictures by text prompt P1 (ship), P2 (chair), P3 (elderly man), P4 (Girl), and P5 (Astronauts); the full-text prompt is shown in the caption of Fig. 9. We can see that, our LCM-LoRA (GAND) still maintain generability, this is a surprising result.

⁵<https://huggingface.co/docs/diffusers/api/schedulers/lcm>



Figure 9: P1: A gorgeous ship sails under a beautiful starry sky. P2: Cradle chair, a huge feather, sandy beach background, minimalism, product design, white background, studio light, 3d, iso 100, 8k. P3: In a serene, snowy landscape, an elderly man in a straw raincoat and hat fishes alone on a small wooden boat in a calm, cold river. Surrounded by snow-covered trees and mountains, the tranquil scene conveys harmony with nature and quiet isolation. Masterpiece. Chinese art. extreme details. P4: Self-portrait oil painting, a beautiful cyborg with golden hair, 8k. P5: Astronauts in a jungle, cold color palette, muted colors, detailed, 8k

Image quality assessment

We also conduct a series of IQAs to evaluate the quality of purified images. To be specific, we leverage:

- PSNR: Range set to 1, aligning with PyTorch’s image transformation.
- SSIM⁶ (Wang et al. 2004): Gaussian kernel size set to 11.
- LPIPS⁷ (Zhang et al. 2018): Utilizing VGG (Simonyan and Zisserman 2015b) as the surrogate model.

It is worth noting that, we borrow the implementation of PSNR from TorchEval⁸.

	LPIPS↓	PSNR↑	SSIM↑
$IQA(\mathbf{x}, \mathbf{x}_{adv})$	0.1547	34.21	0.8906
$IQA(\mathbf{x}, \mathbf{x}_{ours})$	0.2370	24.13	0.7343
$IQA(\mathbf{x}, \mathbf{x}_{DiffPure})$	0.2616	24.11	0.7155

Table 10: IQAs for $\epsilon = 8/255$. ↑/↓ indicate higher/lower value consists the better image quality. Notably, $IQA(\cdot)$ indicates one of IQA we leverage, \mathbf{x} refers to the clean image, \mathbf{x}_{adv} refers to the adversarial sample, \mathbf{x}_{ours} refers to the purified image by our method and $\mathbf{x}_{DiffPure}$ refers to purified image by DiffPure.

In Tab. 10, we test the IQA performance of our method on a subset of 1000 pictures randomly sampled from ImageNet, compared with DiffPure, as known as the current SOTA method. We define the same t^* for both methods, both t^* are set as 250. As shown in the table, our LPIPS loss, measures how different the two images are, compared with the original image is smaller than DiffPure, which reduces from 0.2616 to 0.2370. For PSNR and SSIM, which measure the similarity of images. Our methods have higher performance in PSNR and SSIM, increasing from 24.11 to 24.13 and 0.7155 to 0.7343, respectively. This result shows that our method is more similar to the original image, which makes our method have better purification results.

⁶<https://github.com/Po-Hsun-Su/pytorch-ssim>

⁷<https://github.com/richzhang/PerceptualSimilarity>

⁸<https://pytorch.org/torcheval/stable/>